# Integrated Remote Sensing Imagery and Two-dimensional Hydraulic Modeling Approach for Impact Evaluation of Flood on Crop Yields

Huili Chen[1], Zhongyao Liang[1], Yong Liu [1*],Qiuhua Liang[2], Shuguang Xie[1]

1. College of Environmental Science and Engineering, Key Laboratory of Water and Sediment Sciences (MOE), Peking University, Beijing 100871, China.

2. School of Civil Engineering and Geosciences, Newcastle University, UK

* Corresponding Author:

E-mail: yongliu@pku.edu.cn (Y. Liu); TEL: 86 10 62753184; FAX: 86 10 62751927.

# ABSTRACT

The projected frequent occurrences of extreme flood events will cause significant losses to crops and will threaten food security. To reduce the potential risk and provide support for agricultural flood management, prevention, and mitigation, it is important to account for flood damage to crop production and to understand the relationship between flood characteristics and crop losses. A quantitative and effective evaluation tool is therefore essential to explore what and how flood characteristics will affect the associated crop loss, based on accurately understanding the spatiotemporal dynamics of flood evolution and crop growth. Current evaluation methods are generally integrally or qualitatively based on statistic data or ex-post survey with less diagnosis into the process and dynamics of historical flood events. Therefore, a quantitative and spatial evaluation framework is presented in this study that integrates remote sensing imagery and hydraulic model simulation to facilitate the identification of historical flood characteristics that influence crop losses. Remote sensing imagery can capture the spatial variation of crop yields and yield losses from floods on a grid scale over large areas; however, it is incapable of providing spatial information regarding flood progress. Two-dimensional hydraulic model can simulate the dynamics of surface runoff and accomplish spatial and temporal quantification of flood characteristics on a grid scale over watersheds, i.e., flow velocity and flood duration. The methodological framework developed herein includes the following: (a) Vegetation indices for the critical period of crop growth from mid-high temporal and spatial remote sensing imagery in association with agricultural statistics data were used to develop empirical models to monitor the crop yield and evaluate yield losses from flood; (b) The two-dimensional hydraulic model coupled with the SCS-CN hydrologic model was employed to simulate the flood evolution process, with the SCS-CN model as a rainfall-runoff generator and the two-dimensional hydraulic model implementing the routing scheme for surface runoff; and (c) The spatial combination between crop yield losses and flood dynamics on a grid scale can be used to investigate the relationship between the intensity of flood characteristics and associated loss extent. The modeling framework was applied for a 50-year return period flood that occurred in Jilin province, Northeast China, which caused large agricultural losses in August, 2013. The modeling results indicated that (a) the flow velocity was the most influential factor that caused spring corn, rice and soybean yield losses from extreme storm event in the mountainous regions; (b) the power function archived the best results that fit the velocity-loss relationship for mountainous areas; and (c) integrated remote sensing imagery and two-dimensional hydraulic modeling approach are helpful for evaluating the influence of historical flood event on crop production and investigating the relationship between flood characteristics and crop yield losses.

**KEYWORDS:** Yield Loss; Flood Characteristics; Remote Sensing; Two-dimensional Hydraulic Model; HJ-1A/B Imagery

## 1 INTRODUCTION

Floods are one of the most frequent and devastating agricultural hazards (UNDP, 2004), which often cause severe crop production losses (Schmidhuber & Tubiello, 2007) and threaten food security (Kenyon et al., 2008; MRC, 2011). Meanwhile, climate change is expected to generate more challenges in the management of agricultural floods (IPCC, 2013; Lu et al., 2016). The losses from floods to agricultural production are likely to be greater under future climate scenarios. To alleviate potential crop losses from floods, quantitative and spatial assessment of agricultural flood loss and the relationship between flood characteristics and crop failure are essential prerequisites for providing some helpful and targeted guidance. Thus, it is imperative to establish a scientific evaluation system of agricultural flood influence, considering the temporal and spatial characteristics of flood.

Recently, flood loss evaluation to agriculture has gained considerable attention for its contribution to helping stakeholders make informed decisions. Two methods have been developed for flood damage estimation. One is based on ex-post surveys of affected populations and assets to estimate losses, which is time-consuming and strenuous. The other approach employs what is known as “loss functions”, which describes the relationship between flood intensity and the associated loss extent (Kwak et al., 2015; Karagiorgos et al., 2016). Flood intensity can be represented by flood hazard parameters, including water depth, flow velocity, flood duration, etc. The formation of loss functions is the most important procedure in the formation of the latter method. The loss functions can be derived based on historical loss data, questionnaire surveys and experimental evidence. Historical loss data from actual flood events can be used to derive historical loss functions, which can be a guide for future events. However, historical flood damage data are generally scarce and hardly available (Vozinaki et. al., 2015). Some studies construct loss functions with questionnaire surveys relying on the expertise of local experts in the farming industry (Brémond et al., 2010; Vozinaki et al., 2015; Chau et al., 2015). Furthermore, some researchers concentrate on laboratory testing under controlled flood characteristics (Ganji et al., 2012; Anandan et al., 2015). Such experiments are very difficult to conduct and challenging to extrapolate the laboratory findings to different places since there are lots of differences from place to place. Moreover, the loss functions method has limitations for effective risk assessment because of the poor availability of spatial data of flood characteristics, such as inundation duration and flow velocity. Due to the above limitations, a looming question is the following: is it possible to develop a spatial evaluation framework of agricultural flood influence? Considering the effects of flood characteristics and the spatial distributions of floods and crops, the proposed method should have the ability to cover spatial variation and to predict flood progress.

Remote sensing has proven to be a valid tool for monitoring the spatial variation of crop growth dynamics and yield (Beckerreshef et al., 2010; Zhang & Zhang, 2016). The National Oceanic and Atmospheric Administration (NOAA) Advanced Very High Resolution (AVHRR) and Moderate Resolution Imaging Spectroradiometer (MODIS) are the most widely employed spatial data in crop yield monitoring due to their wider coverage, relatively longer data archive and daily observation. However, the AVHRR and MODIS resolutions are coarse and face the problem of classification uncertainties due to mixed types of land cover, especially on highly fragmented fields (Dong & Xiao, 2016; Zhong et al., 2016). Higher spatial resolution remote sensing data, e.g., Landsat TM/ETM+, SPOT, have been demonstrated to be promising in capturing small-patch farmland. However, their relatively longer observation periods prevent effective monitoring of crop growth dynamics. As a part of the project "*Environmental and Disaster Monitoring and Forecasting with a Small Satellite Constellation (HJ-1)*" in China, two small optical satellites (HJ-1A and HJ-1B) were launched on September 6, 2008. The charge-coupled device (CCD) cameras of these satellites have a 30-m spatial resolution and a two-day revisiting period (Wang et al., 2010). The high temporal resolution and mid-high spatial resolution of HJ-1A/B enable the availability of monitoring the dynamics of small-patch fields and are appropriate for monitoring damage from floods. Thus, we attempted to evaluate the spatial variation of crop yields and yield losses from flood using HJ-1A/B imagery and other auxiliary information.

As an overwhelming storm disaster, floods can be highly localized due to the effect of both weather and topography (Thornton et al., 2014), and flood characteristics in watersheds possess highly spatial and temporal heterogeneity. Remote sensing imagery has become an ideal tool for effectively incorporating the spatial extent of flood inundation in loss evaluation (Pantaleoni et al., 2007; Kwak et al., 2015; Kotera et al., 2016). However, these data are unable to provide information on the spatial and temporal characteristics of other parameters, such as flow velocity and flood duration. Recently, advanced two-dimensional hydraulic model has accomplished spatial and temporal quantification of these flood parameters in watersheds (Nguyen et. al., 2015; Bellos et. al., 2016). This type of hydraulic model requires high-quality input data, especially terrain data (Bates et al., 1998; Callow et al., 2007; Schumann et al., 2014). Recent progress in remote sensing can provide the required terrain data for flood simulation (Sanders, 2007; Tarekegn et al., 2010; Baugh et al., 2013; Jarihani et al., 2015; Samantaray et al., 2015; Fernández et al., 2016). For efficient and high-resolution simulation of large-scale areas using two-dimensional hydraulic model, the high computational demand will be the most challenging task. The development of Graphics processing unit (GPU) for high-performance parallel computing can effectively solve the problem of huge computational cost and can enable catchment-scale simulations involving millions of computational cells (Lacasta et al., 2015). Thus, the accessibility of terrain data and high-performance computing ability make it possible to obtain elaborate information about flood characteristics at a grid scale over large areas, which can be used to explore the influence of floods on crop growth dynamics.

Therefore, this study aimed to develop an integrated evaluation framework to investigate the influence of extreme flood event on crop production in Jilin Province with 187,400 km$^2$ of area. Specifically, three questions were asked: (a) what is the spatial variation of crop yield loss extent from flood; (b) what flood parameter is the most influential factor causing crop failure; and (c) what is the relationship between the intensity of most influential factor and associated yield loss extent? The integrated evaluation framework includes the following three steps: (a) Vegetation indices derived from remote sensing imagery with mid-high spatial and temporal resolution were used to monitor the crop yields and evaluate yield losses under extreme flooding; (b) the two-dimensional hydraulic model was employed to simulate the flood dynamics with spatial surface runoff derived from SCS-CN as the input; and (c) the spatial combination of the crop yield loss and flood dynamics on a grid scale was used to investigate the relationship between the intensity of flood characteristics and the associated loss extent. The modeling framework was applied to a 50-year return period flood event that occurred in Jilin Province, in northeastern China, which caused huge agricultural losses in August of 2013.

# 2 MATERIALS AND METHODS

## 2.1 Study Area and the Flood Event

Jilin Province (northeastern China), one of the most important agricultural areas of China, was selected as a case study to explore the regional effect of flood characteristics on crop production. Its climate is dominated by a continental monsoon climate, i.e., the rainy season (July to September) overlaps with the crop-growing season (April to September). The annual average precipitation spatially varies from approximately 350 mm in the northwest to over 1500 mm in the southeast. In this region, agriculture is occasionally disturbed by flooding. Meanwhile, Jilin is a major agricultural province, and its commercial volume of agricultural products and grain per capita have been at the forefront in China in recent years. Jilin is located in the famous black soil belt and is ideal for producing spring corn, soybean and rice, which are the three major crops of Jilin. It produces half of the commercial corn and approximately 14% of the total production in China. Jilin is one of the main provinces producing rice in northern China. Its planting area and rice production have increased in recent years. Furthermore, the midwestern Jilin is suitable for planting soybeans, and its soybean planting area ranks third in China. Accordingly, this study focused on the production conditions and yield losses of spring corn, soybean and rice.

From the 14th to 30th of August 2013, an extreme flood event hit the northeastern part of China producing disastrous consequences for the provinces of Heilongjiang, Jilin and Liaoning. The flood was estimated to be a 50-year return period flood (Jin et al., 2015). According to the Ministry of Civil Affairs, approximately 5 million people were affected, killing 95 people, collapsing 11,530 rooms in houses and damaging 154,622 rooms; and 1.59 million hectares of croplands were affected (Branch of the Red Cross Society of China, 2013). The flood occurred in August, during the crucial growth stages of three major crops, i.e., the silking stage for spring corn, the heading stage for rice and the podding stage for soybeans, thus resulting in extremely severe agricultural losses.

Two typical agricultural watersheds, i.e., the headwater watersheds of the Dongliao River and Mudanjiang River, were identified for investigating how flood characteristics influence crop failure (Fig. 1). The headwater watershed of the Dongliao River (HDL) is in Liaoyuan City, in Jilin Province, where spring corn and rice are intensively cultivated. HDL covers an area of approximately 2191 km$^2$ and approximately 49% is arable land. The elevation is between 58 m and 869 m. The mean annual precipitation of HDL is approximately 666 mm. Rainfall is variable in timing, with 80% of rainfalls occurring during the summer and autumn. The mean annual temperature is 5.25℃. The headwater watershed of the Mudanjiang River (HMU) is in Dunhua, in Jilin Province, where soybean is intensively cultivated. HMU covers an area of approximately 2953 km$^2$ and 165 km$^2$ is planted soybean. The elevation of HMU is between 169 m and 1721 m. It possesses significant mountain climate characteristics. The total annual rainfall is approximately 550–630 mm, and the mean annual temperature is 2.9℃.

## 2.2 Integrated Methodological Framework for Flood Impact Evaluation

An evaluation framework was proposed for analyzing the regional impact of floods on crop production (Fig. 2). Five main steps were proposed as below:

(1) Crop Pattern Identification. The HJ-1 A/B CCD imagery is appropriate for distinguishing crop types and was selected based on the reflection characteristics of each crop; the supervised

maximum likelihood classifier was applied to produce the crop pattern map.

(2) Yield Loss Evaluation. Based on the crop pattern map, vegetation indices for each crop at different growth stages were derived from multi-temporal HJ-1 A/B CCD imagery. Vegetation indices in association with agricultural statistics data were used to develop empirical models to monitor the crop yield and evaluate the yield loss from flood.

(3) Surface Runoff Generation. The spatial hourly precipitation data were used as the input for the SCS-CN model to generate the hourly surface runoff.

(4) Flooding Characteristics Simulation. The spatial surface runoff derived from SCS-CN was input into the two-dimensional hydraulic model domain and flow routed within the domain before being concentrated at the watershed outlet with the help of GPU parallel computing.

(5) Integrated Analysis. Finally, integrated analysis between yield losses and flood characteristics was carried out to analyze the effect of flood on crop production.

### 2.3 Crop Yield Model Development

To monitor the yield of specific crops and the yield losses under the effects of flood risk, we combined remote sensing imagery and crop statistics to develop empirical regression-based yield models. More information on crop yield prediction by remote sensing can be referred to Atzberger (2013), Calvão & Pessoa (2015) and Xue & Su (2017). The comparison between vegetation indices from remote sensing imagery and the official yield statistics was carried out to derive regression models as follows:

$$y = \sum_{i=1}^{\mathrm{m}} \sum_{j=\mathrm{c}}^{\mathrm{n}} a_{ij} * x_{ij} + \mathrm{b}_0 \tag{1}$$

where $y$ is the crop yield; $x$ is the vegetation index; $i$ represents the vegetation index symbol; $j$ represents the crucial month for crop harvesting from $\mathrm{c}$ to $\mathrm{n}$; $a$ is the regression slopes for models; and $\mathrm{b}_0$ is the model intercept.

In this study, three types of data were used: (a) county-level crop statistics, including crop production, planting area and yield; (b) crop pattern map; and (c) HJ-1A/B surface reflectance data. The crop pattern map was used to identify the crop spatial distribution. The yield statistics were then employed to develop an empirical relationship between the vegetation indices of the identified crop field and the crop yield.

The Jilin Statistics Yearbook collects detailed annual county-level agricultural information across Jilin Province. Crop production (t), planting area (ha) and yield data (t ha$^{-1}$) for spring corn, rice and soybean for 2013 and 2014 were obtained from the Jilin Bureau of Statistics. To quantify the yield loss by the flood of 2013, we used 2014 data, which had no major natural disasters, such as drought, flood, etc., as the benchmark year.

Identification of crop fields is an important step in regression-based model development and implementation as it allows for crop-specific remotely sensed indices. In this study, HJ-1A/B CCD images for the 3rd and 4th of September 2013 were used in a supervised classification model to produce land use classification that distinguished different crop types. It was easy to identify training areas for the three major crops in September when major crops were at different growth stages and had different reflection characteristics. Although the location of crop fields may vary from year to year due to crop rotation, we found that the spatial distribution of the three major crops remained relatively constant between 2013 and 2014 when comparing the HJ-1A/B CCD images of these two years. Therefore, in this study, we employed the same crop pattern map.

We employed HJ-1A/B CCD images at 30 m resolution for every month from July to September. The period from July to September was crucial for crop harvesting, which corresponded to a joint-maturity stage for spring corn, tillering-maturity stage for rice, and flowering- maturity stage for soybean. For every month, we chose the mid-month images for consistency between these two years. However, owing to the effects of clouds, the consistency could not be fully achieved. These images were geometrically corrected based on the images from September 2013 to ensure sub-pixel geolocation accuracy. The Normalized Difference Vegetation Index (*NDVI*) (Tucker, 1979) and Enhanced Vegetation Index (*EVI*) (Huete et al., 2002) were used for crop yield predictions. These two indices were selected according to their popularity and capability for analyzing crop growth dynamics. The formulas for calculating *NDVI* and *EVI* are as follows:

$$NDVI = (R_{Nir} - R_{Red})/(R_{Nir} + R_{Red}) \tag{2}$$

$$EVI = 2.5 \times (R_{Nir} - R_{Red})/(R_{Nir} + 6 \times R_{Red} - 7.5 \times R_{Blue} + 1) \tag{3}$$

where $R_{Nir}$, $R_{Red}$ and $R_{Blue}$ refer to the reflectance of the near-infrared, red and blue bands of HJ-1A/B CCD images, respectively.

The NDVI was the most widely employed index to statistically correlate with crop growth dynamics and yield across the world (Satir & Berberoglu, 2016). More recently, the EVI has proven to be more effective in monitoring crop growth than NDVI (Bernardes et al., 2012; Bolton & Friedl, 2013; Zhang et al., 2014; Johnson, 2016). This is owing to fact that the EVI remains sensitive to variance in dense vegetation when the NDVI becomes saturated. Therefore, we adopted both of them for the sake of more effectively responding to crop growth dynamics.

The crop pattern map was used to retrieve the NDVI and EVI values for the three major crops. The averaged NDVI and EVI for every growth stage of each crop were computed for each county. Then, the linear relationships between NDVI, EVI and the yield statistics were derived for each crop. Considering the inconsistency of daily images for the same month between 2013 and 2014, the crop model was built separately. To obtain these relationships, stepwise linear regression (SLR) was used. SLR enables selection of the relevant variables using the binary relationships between independent and dependent data and reduces the error caused by standard multi-linear regression with inputs of all variables.

### 2.4 Surface Runoff Derived from a Hydrological Model

The SCS-CN model (Woodward et al., 2002) was selected on the basis of its simplicity and success in simulating hydrological processes (Mishra & Singh, 2003; Mishra & Singh, 2012; Zhang & Pan, 2014; Chen et al., 2016). Although Caviedes-Voullième et al. (2012) found that the SCS-CN methods might be unsuitable for shallow-water based hydrological simulation. Infiltration models, such as Horton and Green-Ampt methods may be more suitable to be used together with hydraulic models to predict surface runoff (Fernández-Pato et al., 2016). But these models commonly require substantial field data for model calibration and verification and are not suitable for the current study. Meanwhile this study focus more on the spatial distribution of flood variables' relative value by hydraulic modeling. For these reasons, this study will apply SCS-CN. SCS-CN was designed to compute volume of surface runoff ($SR$) for a specific rainfall event. The SCS-CN method is expressed as follows:

$$SR = \frac{(P - I_a)^2}{(P - I_a) + S} \tag{4}$$

where $P$ is rainfall depth; $S$ is the potential maximum retention; $I_a$ is initial abstraction and $I_a = \lambda S$, with $\lambda$ generally taken as 0.2; the parameter $S$ is related to the Curve Number (CN) as follows:

$$S = \frac{2540}{CN} - 25.4 \tag{5}$$

The value of CN as the only parameter in SCS-CN can be derived from the National Engineering Handbook, Section-4 (SCS, 1956), which considers the catchment characteristics, such as land use, soil type and antecedent soil moisture conditions. In this study, the surface runoff was calculated with SCS-CN for every grid in every time step, using the cumulative precipitation from the beginning of the rainfall event to the given time. Therefore, the cumulative surface runoff was gained for that time. Then, surface runoff was the increment calculated by subtracting the cumulative surface runoff from the previous time step.

As implemented for the selected watersheds, SCS-CN employed a 30 m × 30 m grid, with the cumulative precipitation, antecedent soil moisture, soil type and land use for each cell. The simulation period was from 3 pm on August 15th to 6 am on August 21th 2013, which was the key period for the formation and evolution of this extreme flood event.

SCS-CN simulations were forced using hourly cumulative precipitation data estimated from a network of 86 and 45 precipitation gauge stations for HDL and HMU, respectively (Fig. 1). The hourly precipitation data employed here were the highest temporal resolution data that we can get, which were from the Hydrology Bureau of Jilin Province. The data represented the best density of precipitation stations that can capture the spatial variations of precipitation. Estimates of hourly cumulative precipitation and antecedent soil moisture derived as rainfall over the 5 days before the rainstorm within each SCS-CN grid cell were obtained by interpolating from the four nearest gauges using the inverse distance squared weighting method.

### 2.5 Two-Dimensional Hydraulic Modelling

Outburst floods across the selected watersheds were simulated using shallow water model that conserves mass and momentum by solving the two-dimensional, depth-averaged, shallow-water equations on a rectangular grid. Detailed information can be seen in Hou et al. (2014) and Xia & Liang (2016). The conservative form of the two-dimensional shallow water model is given by the following:

$$\frac{\partial \mathbf{q}}{\partial t}+\frac{\partial \mathbf{f}}{\partial x}+\frac{\partial \mathbf{g}}{\partial y}=\mathbf{s} \tag{6}$$

where $t$ is the time; $x$ and $y$ are the Cartesian coordinates; $\mathbf{q}$ is the flow variable vector; $\mathbf{f}$ and $\mathbf{g}$ denote the flux vectors in the x and y direction, respectively; the $\mathbf{s}$ is the source term vector.

$$\mathbf{q}=\begin{bmatrix} h \\ q_x \\ q_y \end{bmatrix} \qquad \mathbf{f}=\begin{bmatrix} q_x \\ uq_x+\frac{1}{2}gh^2 \\ uq_y \end{bmatrix}$$

$$\mathbf{g}=\begin{bmatrix} q_y \\ vq_x \\ vq_y+\frac{1}{2}gh^2 \end{bmatrix} \qquad \mathbf{s}=\begin{bmatrix} 0 \\ -C_f u\sqrt{u^2+v^2}-gh\frac{\partial z_b}{\partial_x} \\ -C_f v\sqrt{u^2+v^2}-gh\frac{\partial z_b}{\partial_x} \end{bmatrix} \tag{7}$$

where $h$ denotes the water depth; $q_x$ and $q_y$ denote the unit-width discharges in x- and y directions, respectively; $u$ and $v$ are the depth-averaged velocities in x- and y-directions, respectively; and $q_x = uh$ and $q_y = vh$; $z_b$ is the bed elevation; $C_f$ is the bed roughness coefficient.

As implemented for the selected watersheds, the two-dimensional hydraulic model employed a 30 m × 30 m grid, using the surface runoff, DEM and roughness coefficient in each cell as inputs. The time step used for hydraulic simulating is 1 s, which can be adaptively increased according to the local Courant-Friedrichs-Lewy (CFL) condition. In order for depicting the whole flood process, the duration of the simulation was 136 h, which was longer than the rain process (60 h) and the same as the SCS-CN model. The runoff produced during 1 hour of the hydrological scheme is assumed to occur at the same rate over that time step as the input of hydraulic model and the flow was routed within the domain before concentrating at the watershed outlet. The topographic data were derived from ASTER GDEM version 2 developed by the Ministry of Economy, Trade, and Industry of Japan (METI) and the United States National Aeronautics and Space Administration (NASA). The spatial resolution of ASTER GDEM is 30m, which is the finest resolution among all free downloadable topographic data in China. Adequate flood simulations require not only terrain data but also hydraulic roughness data of the earth's surface. The shallow water model performed the bed friction stress with Manning's roughness coefficient ($n$). Numbers of studies estimated the Manning roughness $n$ from a lookup table based on the catchment characteristics and successfully applied them to hydraulic models (e.g., Mtamba et al., 2015; Garrote et al., 2016). There have been various studies that offer Manning lookup tables, e.g., Chow, 1959; Barnes, 1967; Arcement & Schneider, 1984. Thus, we determined the roughness coefficient using the land use types based on these lookup tables. We set $n$=0.016 for urban land, 0.027 for ponds, 0.03 for grassland, 0.035 for cultivated land, and 0.15 for forest.

The necessity that the spatial resolution (30 m) is consistent between the yield loss evaluation and flood simulation requires the use of millions of computational cells (2.43 million for HDL and 2.95 million for HMU), hence there is a high computational cost and increased computational time. To improve the computational efficiency and reduce the computation time, the two-dimensional hydraulic model was carried out on GPU using NVIDIA's parallel computing architecture CUDA (compute unified device architecture).

The model outputs for flood stage and the $x$ and $y$ components for flow velocity were saved as grids every 1 h. The water depth (*h*) was determined by the difference between the flood stage and bed elevation, and the streamwise velocity (*u*) was calculated by the vector sum of the *x* and *y* velocity components. The 136 grids were averaged and maximized. Meanwhile, the durations of water depth exceeding 5 cm, 10 cm and 20 cm for every grid were counted.

# 3 RESULTS AND DISCUSSION

## 3.1 Yield Predictions and Losses based on Flood Evaluation

We used a supervised classification method to produce pattern maps of three major crops for the Jilin Province at the HJ-1A/B 30 m resolution (Fig. 3). To quantitatively validate this map, the classified spring corn, rice and soybean were aggregated to the county scale and compared with the official planted area statistics. When compared at the county level, the classified area for spring corn from the 30 m mask was well correlated with the statistical area (Classified estimate=0.88*statistics area, $R^2$=0.83) (Fig. 4). For rice and corn, the classified results were not as good as spring corn, but they were acceptable ($R^2$=0.80 for rice and $R^2$=0.70 for soybean) (Fig. 4). Hence, spring corn, rice and soybean fields were extracted for yield evaluations from multi-temporal HJ-1A/B datasets.

The NDVI and EVI values for different crops were retrieved by using the crop pattern map as mask. The NDVI and EVI values were averaged by the county level. The relationships between the yield statistics data and vegetation indices at the county level were derived by SLR model to obtain the most descriptive indices for yield development. The yield model equations and variables are presented in the *Supporting Material* (Table S1). The models were derived using SPSS software. From Table S1, the coefficients of determination ($R^2$) were greater than

0.6 for spring corn and soybean. For rice, the $R^2$ for 2013 ($R^2$=0.55) was relatively lower than that of 2014 ($R^2$=0.70). Meanwhile, the SLR results indicate that the most accurate indices for yield prediction were different between the flood year 2013 and the benchmark year 2014. Fig. 5 shows the actual yield and the model predictions. Most of the data points were close to the 1:1 line. On the whole, the results of the empirical models based on vegetation indices can sufficiently capture the yield variation of the three major crops in Jilin.

The predicted yield maps of the three major crops for HDL and HMU watersheds were developed from regression-based models employing different indices presented in Table S1. These maps exhibit obvious spatial variation in yields, as represented by different colors. The yield loss map can be generated using the yield maps of 2013 and 2014. There were no other major natural factors apart from flooding that reduced the yield in 2013 according to officials and local media reports. Hence, we assumed that the reduction in yield from 2013 was caused by the flood. We employed the yield ratio between these two years as the measure of yield loss extent.

Fig. 6 shows the spatial variation of crop yield loss extent from flooding. We can determine the area and extent of yield loss from this rainstorm. For spring corn, approximately 25% of the area displayed yield reductions and the average ratio of yield loss was 12%. The yield loss was more severe in rice. Nearly half of the rice area experienced crop failure, and the average ratio of yield loss was 15%. For soybean, the area percentage of crop failure was 25%, and the average ratio of yield loss was 11%. Meanwhile, crop damaged by floods is mainly concentrated in the low lands around rivers, which are usually more vulnerable to flood attack. If the areas are confined to 500 meters buffer zones around river networks, the relative damage is obviously higher than the whole catchment. For spring corn, 33% of the area displayed yield reductions and the average ratio of yield loss was 19% in the buffer zones; for rice and soybean, the area percentage of crop failure was 59% and 28%, and the average ratio of yield loss was 17% and 20%, respectively. Taken together, this flood event resulted in a considerable reduction in crop yield, especially for the potential vulnerable areas.

Because remote sensing devices can concurrently monitor large-scale areas and observe the same location at regular intervals, remote sensing imagery has been employed to assess the impact of floods and other natural disasters. In particular, remote sensing imagery provides vegetative index measure, wherein the impact of flooding on agricultural crops can be quantified. The HJ-1 A/B CCD imagery can avoid classification uncertainty resulting from mixed pixels of coarse resolution satellite data and provides the possibility for more accurate and detailed description of the spatiotemporal dynamics of crop biophysical variables. Successful exploitation of the vegetation indices based on multi-temporal HJ-1 A/B CCD imagery can help us determine the spatial variation of crop yield and evaluate the yield loss from floods at a high spatial resolution over large areas (Fig. 6).

### 3.2 Flood Simulation Results

We coupled the two-dimensional hydraulic model with the SCS-CN hydrological model for flood simulation in 30-m resolution grid. The coupled framework used SCS-CN as a rainfall-runoff generator and ran the routing scheme with the hydraulic model to predict grid-based and time-varying flood depths and velocities for the entire basin. The rainfall hyetographs and surface runoff from SCS-CN are shown in in the *Supporting Material* Fig. S1. Figs. 7, 8 and S2 displayed the distributed high-resolution flow information for the HDL and HMU basin, respectively. The information included the maximum water depth, mean water depth, maximum flow velocity, mean flow velocity and duration of water depth above 5 cm, 10 cm, and 20 cm. In this study, the input runoff of every time step (1 s) in hydraulic modeling is generally less than 1 mm, thus 1 mm can be used to discriminate the inputed runoff and accumulated water flow, i.e., non-wet (maximum water depth $<$ 1 mm) and wet (maximum water depth $\geq$ 1 mm).

In the HDL basin, the areal average value of antecedent rainfall, i.e., the rainfall over the five days prior to the rainstorm, was 6.27 mm. The cumulative precipitation spatially ranged from 37 mm to 217 mm inside the basin during this flood event. The areal average value of precipitation was 171.28 mm. Total runoff volume from SCS-CN is 96404,000 $m^3$, and the measured volume is 106999,560 $m^3$ from the Quantai station, which is near the watershed outlet. The error between the measured volume and computed volume is 10%, thus the result from SCS-CN is acceptable. According to the simulation results (Fig. 7), 41% of the watershed area was wet. The average depth and maximum depth in the wet area was 0.014 m and 0.092 m, respectively. The maximum flow velocity spatially varied from 0 m/s to 1.98 m/s. Moreover, 4.8%, 4.4% and 3.9% of the area was wet by over 5 cm, 10 cm and 20 cm, respectively. In the HMU basin, the areal average value of antecedent rainfall was 9.81 mm. The cumulative precipitation spatially varied from 0 mm to 172 mm during the flood. The areal precipitation was 76.12 mm. Total runoff volume from SCS-CN is 62308,300 $m^3$, the measured volume is 73839,407 $m^3$ from the Xiwaizi station at watershed outlet. The error between the measured volume and computed volume is 16%, thus the result from SCS-CN is acceptable. From the simulation results (Fig. 8), 35% of the watershed area was wet. The average of depth and maximum depth in the flooded area was 0.016 m and 0.034 m, respectively. The maximum flow velocity spatially varied from 0 m/s to 2.89 m/s. Moreover, 4.4%, 2.5% and 1.4% of the area was wet by over 5cm, 10cm and 20cm respectively.

The simulation results of the two-dimensional hydraulic model provide a clear picture of the flood characteristics for the entire basin, yet maintain a high enough spatial resolution so that the flooding effect on individual fields, which is highly localized, can be observed (Fig. 7 and Fig. 8). In this study an individual field area is 900 m$^2$ (30*30m), which is spatial size of computational cell for hydrodynamic modeling. While some existing hydraulic models are capable of depicting complex surface flow, it often only includes the river reach (e.g., Bonnifait et. al., 2009), small catchments (Kim et. al., 2012) or low-resolution data (Neal et. al., 2012; Paiva et. al., 2013) due to computational expense. The hydraulic model, with the help of GPU parallel computing allows for efficient production of flow information at high spatial resolutions for the whole catchment. The water depth and flow velocity are very important information for flood warning and can potentially be used to deepen the understanding of associated disasters.

### 3.3 Evaluation of Flood Characteristics on Crop Yield Losses

After accomplishing the yield loss evaluation based on remote sensing imagery and flood simulation via hydraulic modeling, the yield loss ratio and flood characteristics can be gained detailedly for every cell. Then we counted the average value of flood variables (including the water depth, flow velocity, and duration at depth above 5 cm, 10 cm, and 20 cm) for cells with the same yield loss ratio. Thus we can gain the average value of flood variables against every 1% yield loss ratio. The relationships between the flood characteristics and yield loss ratio are presented in Table 1 and Figs. S3, S4, and S5. The flood characteristics include the water depth, flow velocity, and duration at depth above 5 cm, 10 cm, and 20 cm.

### 3.3.1 The Most Influential Factor that Caused Crop Failure

According to the yield loss evaluation based on multi-temporal HJ-1 A/B CCD imagery, 62690 cells for corn, 4416 cells for rice, and 44960 cells for soybean displayed yield reductions. We counted the average value of flood variables from these abundant cells with having the same yield loss ratio, i.e., the corresponding average values of flood variables in every 1% yield loss ratio. Then we investigated the relationships between the flood variables and yield loss ratio. For spring corn, the water depth, flow velocity and duration were all negatively correlated with yield loss (Table 1). The correlations with maximum flow velocity peaked at the highest level, with a Pearson's coefficient (r) of -0.86. There was little difference between the maximum flow velocity and mean flow velocity. The water depth was weaker, with an r of around -0.6 and the mean water depth was slightly stronger than the maximum's. The durations of the flood exhibited the weakest value among all of the parameters. For rice, the water depth, velocity and duration were all negatively correlated with yield loss. The mean flow velocity had the strongest negative correlation, reaching -0.78. There was no obvious difference between the maximum and mean flow velocity. The mean water depth had a greater effect than the maximum water depth. Meanwhile, the duration with depths greater than 20 cm was stronger than that of 5 cm and 10 cm. Furthermore, the r of duration with depths >20 cm and the mean water depth were almost equal. For soybean, the overall results were similar to spring corn and rice in that all seven flood characteristics were negatively correlated with yield lose. The mean flow velocity presented the strongest negative correlation, reaching -0.70. And the mean flow velocity was superior to the maximum flow velocity. The duration was weaker, with r varying from -0.28 to

-0.51. Moreover, the water depth exhibited the weakest correlation, with an r of just -0.1. It should be noted that we adopted the average values to investigate the most relevant variable and the factor-loss functions. The average values help us simplify data analysis from the large amount of cells affected by flood and more easily capture the key factor, however, they may result in underestimation of the flood variables, which influences the numerical relationship between the factor and yield loss. Thus the factor-loss functions are not exactly physical factor-loss functions, and should be carefully treated.

Based on the above results, the maximum flow velocity is the most influential factor on spring corn at silking stage corresponding to the flood occurrence period and the mean flow velocity for rice at the heading stage and for soybean at the podding stage. The HDL and HMU are in the river source areas and have steep terrain, where the average slope of HDL and HMU are 8.3° and 9.3°, respectively. In these steep mountainous regions, flash floods are commonly characterized by speed-varying surface flow as a result of rapid catchment response to rainfall from intense thunderstorms (Borga et. al., 2014), which results in a short lead time and considerable damage due to high flow velocity (Xia et. al, 2011; Karagiorgos et. al., 2016). Thus, the crop yield loss was more strongly correlated with the flow velocity than the water depth and duration for HDL and HMU. The higher the flow velocity from flooding, the more likely the agricultural damage. Vozinaki et. al., (2015) collected opinions of practicing and research agronomists and found that flow velocity was a very important damage factor on tomatoes and green vegetables. Ganji et.al, (2012) found that the flow velocity had obvious damage on rice production in a set of laboratory tests. Therefore, in areas with large flow motion, agricultural activity should more carefully consider the potential consequences of extreme flood events.

Reasonable estimation of flood damage is a complex task, especially in the case of flash floods. The identification of suitable flood parameters is of great importance for the realistic assessment of direct crop flood damages and in helping make informed decisions about the management of crop flood risk and food production (Brémond et. al., 2013). The current literature pays more attention to two variables, i.e., water depth (Brémond et. al., 2013; Chau et. al., 2014; Samantaray et. al., 2014) and the duration of floods (Dutta et. al., 2003). The intensive focus on water depth as the main determinant parameter for flood damage might be due to the limited information about other parameters, e.g., flow velocity (Kreibich et. al., 2009). However, a strong influence from flow velocity on crop loss was identified for the two mountainous watersheds in this study. Thus more variables, including the flow velocity, and the flood types and differences, should be taken into account in future research.

### 3.3.2 Relationship between Most Influential Factor and Yield Loss

Based on the above analysis, the r of the most relevant flood parameters for the three major crops were no weaker than -0.7. They showed favorable and satisfactory results, which can help us understand and establish a flood factor-loss function for specific crops in a given environment. In previous studies, the relationships between flood characteristics and the extent of agricultural flood damage are empirical and simple, i.e., grading or linear. According to the observations (Fig. 9), the relationship between the most relevant parameters and the yield lose ratio was nonlinear; that is, they did not decrease at the same rate. The coefficients of determination ($R^2$) indicated that the power function archived the best results among the commonly used functions, such as the linear function, exponential function, power function and logarithmic function. The $R^2$ of the power functions were 0.86, 0.64, and 0.55 for spring corn, rice and soybean, respectively. The power function has an asymptote that is parallel to the “x” axis, which means, after a specific upper limit, there are large increases in the hydraulic parameter that bring about a negligible increase in the loss. The implication is that power function is compatible with realistic condition. Therefore, the power function can be selected as the appropriate functional form for agricultural flood loss estimation. However, one point should be noted: because the results in Fig. 9 were derived from a large number of points across the watershed and represent the average and overall response to floods, they are different from the physical factor-loss functions.

Extreme precipitation is inescapable, but the lessons learned from past practice can be applied to reduce the damage they may inflict. Considering that historical flood damage data are rarely available or restricted in use (Vozinaki et. al., 2015), we explored the relationship between flood intensity and associated crop loss extent by combing the monitoring of remote sensing imagery and the model simulation of floods. According to the analysis, enhancing and developing crop flood management projects should be needed primarily in areas with high flow velocity for mountainous headwater watersheds. Simultaneously based on the flood simulation results of HDL and HMU, we found that the areas with a large topographic slope and relatively low terrain compared to the surrounding environment are more likely to be disturbed by high flow velocity, such as the foot of the mountain and the gorge areas. In order for displaying the velocity more clearly, the local map for the headwater watershed of the Mudanjiang River is showed in the *Supporting Material* Fig S6. It is easy to understand that a large topographic slope can accelerate the motion of water flow, and relatively low terrain can accumulate more water from the surrounding environment, both of which can bring up high flow velocity.

This study integrates the crop yield losses evaluated by remote sensing imagery and flood dynamic characteristics simulated by the two-dimensional hydraulic model to explore the effect of flood on crop production and the relationship between flood intensity and associated crop loss extent. In consideration of the main feature of the hydraulic model that it can depict surface flow based on the conservation of mass and momentum, minimal parameters and successful application in previous studies, no validation works are carried out in this study. Further investigation, such as confirmation with the observed water level and inundation extent derived from remote sensing imagery, are still needed to validate the flood simulation results. The parametrization of rainfall losses by SCN-CN is based on the underlying surface characteristics in combination with previous research, and the sensitivity of results to variations in the parametrization is not investigated in this study considering that the simulation errors by SCS-CN are acceptable. It must be noticed, however, the variations in the parametrization may influence the results about the relationship between flood and yield loss. Further work are still needed to explore the uncertainty of the results and sensitivity to the parametrization in the methodological framework.

## 4 CONCLUSIONS

The remote sensing data and two-dimensional hydraulic model were integrated in this study to facilitate the identification of flood characteristics from an extreme flood event effect on the yield of spring corn, rice and soybean in Jilin Province (China). The modeling results indicated the following：

(a) The empirical models developed from NDVI and EVI for critical periods of crop growth from multi-temporal HJ-1 A/B CCD imagery, in association with agricultural statistical data, can sufficiently capture the yield variation and monitor the spatial variation of yields of spring corn, rice and soybean in Jilin Province.

(b) The August 2013 catastrophic flood affected 25% of the spring corn area, with an average 12% yield reduction, and nearly half of the rice area was affected, with an average 15% yield reduction in the headwater watershed of the Dongliao River; the 2013 flood damaged 25% of the soybean area, with 11% yield losses in the headwater watershed of the Mudanjiang River.

(c) The simulation results of the two-dimensional hydraulic model, with the help of GPU parallel computing, provide a clear picture of the flood characteristics for the entire HDL and HMU, and maintain a high enough spatial resolution (30 m).

(d) For steep mountainous areas, the flow velocity was the most influential factor that caused crop yield losses during the extreme flood event, and the power loss functions archived the best results among the commonly-used functions. For spring corn at the silking stage, the maximum flow velocity is the key factor and the $R^2$ of power loss function was 0.85. For rice at the heading stage and soybean at the podding stage, the mean flow velocity was more important and the $R^2$ of the power loss functions were 0.63 and 0.52, respectively.

## ACKNOWLEDGMENTS

This paper was supported by the National Basic Research Program of China (2015CB458900).

## REFERENCES

Anandan, A., Pradhan, S. K., Das, S. K., Behera, L., & Sangeetha, G. (2015). Differential responses of rice genotypes and physiological mechanism under prolonged deepwater flooding. *Field Crops Research, 172*, 153-163.

Arcement, G. J., & Schneider, R. (1984). Guide for selecting manning's roughness coefficients for natural channels and floodplains. *Roughness Coefficient*.

Atzberger, C. (2013). Advances in remote sensing of agriculture: Context description, existing operational monitoring systems and major information needs. *Remote Sensing, 5*(2), 949-981.

Barnes, H. H. (1967). Roughness characteristics of natural channels. *Center for Integrated Data Analytics Wisconsin Science Center*.

Baugh, C. A., Bates, P. D., Schumann, G., & Trigg, M. A. (2013). SRTM vegetation removal and hydrodynamic modeling accuracy. *Water Resources Research, 49*(9), 5276–5289.

Bates, P. D., Horritt, M., & Hervouet, J. M. (1998). Investigating two-dimensional, finite element predictions of floodplain inundation using fractal generated topography. *Hydrological processes*, *12*(8), 1257-1277.

Beckerreshef, I., Vermote, E., Lindeman, M., & Justice, C. (2010). A generalized regression-based model for forecasting winter wheat yields in Kansas and Ukraine using MODIS data. *Remote Sensing of Environment, 114*(6), 1312-1323.

Bellos, V., & Tsakiris, G. (2016). A hybrid method for flood simulation in small catchments combining hydrodynamic and hydrological techniques. *Journal of Hydrology, 540*, 331-339.

Bernardes, T., Moreira, M. A., Adami, M., & Giarolla, A. (2012). Monitoring biennial bearing effect on coffee yield using MODIS remote sensing imagery. *Remote Sensing, 4*(9), 3760-3763.

Bolton, D. K., & Friedl, M. A. (2013). Forecasting crop yield using remotely sensed vegetation indices and crop phenology metrics. *Agricultural & Forest Meteorology, 173*(2), 74-84.

Bonnifait, L., Delrieu, G., Lay, M. L., Boudevillain, B., Masson, A., & Belleudy, P., et al. (2009). Distributed hydrologic and hydraulic modelling with radar rainfall input: reconstruction of the 8–9 September 2002 catastrophic flood event in the Gard region, France. *Advances in Water Resources*, *32*(7), 1077-1089.

Borga, M., Stoffel, M., Marchi, L., Marra, F., & Jakob, M. (2014). Hydrogeomorphic response to extreme rainfall in headwater systems: flash floods and debris flows. *Journal of Hydrology, 518*(4), 194-205.

Branch of the Red Cross Society of China, (2013). China Floods 2013: Work Report 4. Retrieved August 30, 2013, from http://www.redcross.org.hk/en/disasterrelief_prepard/appeal_update_detail.html?year=2013&id=1654.

Brémond, P., & Grelot, F. (2010). Comparison of a systemic modelling of farm vulnerability and classical methods to appraise flood damage on agricultural activities. In *11th Biennal Conference of the International Society for Ecological Economics (ISEE) Advancing Sustainability in a Time of Crisis*.Brémond, P., Grelot, F., & Agenais, A. L. (2013). Review article: economic evaluation of flood damage to agriculture - review and analysis of existing methods. *Natural Hazards & Earth System Sciences, 13*(10), 2493-2512.

Callow, J. N., Niel, K. P. V., & Boggs, G. S. (2007). How does modifying a DEM to reflect known hydrology affect subsequent terrain analysis?. *Journal of Hydrology, 332*(1–2), 30-39.

Calvão, T., & Pessoa, M. F. (2015). Remote sensing in food production-a review. *Emirates Journal of Food and Agriculture, 27*(2), 138.

Caviedes-Voullième, D., García-Navarro, P., & Murillo, J. (2012). Influence of mesh structure on 2d full shallow water equations and SCS Curve number simulation of rainfall/runoff events. *Journal of Hydrology, s 448–449*(2), 39-59.

Chau, V. N., Cassells, S., & Holland, J. (2015). Economic impact upon agricultural production from extreme flood events in Quang Nam, central Vietnam. *Natural Hazards, 75*(2), 1747-1765.

Chen, L., Wei, G., & Shen, Z. (2016). Incorporating water quality responses into the framework of best management practices optimization. *Journal of Hydrology, 541*, 1363-1374.

Chow, V.T., 1959. Open-channel Hydraulics. McGraw-Hill, Book Co., New York, p. 680.

Dong, J., & Xiao, X. (2016). Evolution of regional to global paddy rice mapping methods: a review. *ISPRS Journal of Photogrammetry & Remote Sensing, 119*, 214-227.

Dutta, D., Herath, S., & Musiake, K. (2003). A mathematical model for flood loss estimation. *Journal of Hydrology, 277*(1–2), 24-49.

Fernández, A., Najafi, M. R., Durand, M., Mark, B. G., Moritz, M., & Jung, H. C., et al. (2016). Testing the skill of numerical hydraulic modeling to simulate spatiotemporal flooding patterns in the Logone floodplain, Cameroon. *Journal of Hydrology, 539*, 265-280.

Fernández-Pato, J., Caviedes-Voullième, D., & García-Navarro, P. (2016). Rainfall/runoff simulation with 2D full shallow water equations: sensitivity analysis and calibration of infiltration parameters. *Journal of Hydrology, 536*, 496-513.

Ganji, Z., Shokoohi, A., & Samani, J. M. V. (2012). Developing an agricultural flood loss estimation function (case study: rice). *Natural Hazards, 64*(1), 405-419.

Garrote, J., Alvarenga, F. M., & Díez-Herrero, A. (2016). Quantification of flash flood economic risk using ultra-detailed stage–damage functions and 2-d hydraulic models. *Journal of Hydrology, 541*, 611-625.

Hou, J., Simons, F., Liang, Q., & Hinkelmann, R. (2014). An improved hydrostatic reconstruction method for shallow water model. *Journal of Hydraulic Research, 52*(3), 432-439.

Huete, A., Didan, K., Miura, T., Rodriguez, E. P., Gao, X., & Ferreira, L. G. (2002). Overview of the radiometric and biophysical performance of the MODIS vegetation indices. *Remote Sensing of Environment, 83*(1-2), 195-213.

IPCC, 2013. Climate Change 2013: The Physical Science Basis. Cambridge University Press, Cambridge, 624–627.

Jarihani, A. A., Callow, J. N., Mcvicar, T. R., Niel, T. G. V., & Larsen, J. R. (2015). Satellite-derived digital elevation model (DEM) selection, preparation and correction for hydrodynamic modelling in large, low-gradient and data-sparse catchments. *Journal of Hydrology, 524*, 489-506.

Jin, C., Li, W., & Li, X. (2015). Research and thinking of flood forecast in Northeast China. *Water Resources & Hydropower of Northeast China, 33(12),* 38-41. (In Chinese)

Johnson, D. M. (2016). A comprehensive assessment of the correlations between field crop yields and commonly used MODIS products. *International Journal of Applied Earth Observation & Geoinformation, 52*, 65-81.

Karagiorgos, K., Thaler, T., Heiser, M., Hübl, J., & Fuchs, S. (2016). Integrated flash flood vulnerability assessment: insights from East Attica, Greece. *Journal of Hydrology, 541*, 553-562.

Kenyon, W., Hill, G., & Shannon, P. (2008). Scoping the role of agriculture in sustainable flood management. *Land Use Policy, 25*(3), 351-360.

Kim, J., Warnock, A., Ivanov, V. Y., & Katopodes, N. D. (2012). Coupled modeling of hydrologic and hydrodynamic processes including overland and channel flow. *Advances in Water Resources, 37*(1), 104-126.

Kotera, A., Nagano, T., Hanittinan, P., & Koontanakulvong, S. (2016). Assessing the degree of flood damage to rice crops in the Chao Phraya delta, Thailand, using MODIS satellite imaging. *Paddy and Water Environment, 14*(1), 1-10.

Kreibich, H., Piroth, K., Seifert, I., Maiwald, H., Kunert, U., & Schwarz, J., et al. (2009). Is flow velocity a significant parameter in flood damage modelling?. *Natural Hazards & Earth System Sciences, 9*(5), 1679-1692.

Kwak, Y., Shrestha, B. B., Yorozuya, A., & Sawano, H. (2015). Rapid damage assessment of rice crop after large-scale flood in the Cambodian floodplain using temporal spatial data. *IEEE Journal of Selected Topics in Applied Earth Observations & Remote Sensing, 8*(7), 3700-3709.

Lacasta, A., Morales-Hernández, M., Murillo, J., & García-Navarro, P. (2015). Gpu implementation of the 2d shallow water equations for the simulation of rainfall/runoff events. *Environmental Earth Sciences*, *74*(11), 7295-7305.

Lu, Y., Qin, X. S., & Xie, Y. J. (2016). An integrated statistical and data-driven framework for supporting flood risk analysis under climate change. *Journal of Hydrology, 533,* 28-39.

Mishra, S. K., & Singh, V. P. (2003). Soil conservation service curve number (SCS-CN) methodology. *Water Science & Technology Library, 22*(3), 355-362.

Mishra, S. K., & Singh, V. P. (2012). Special issue on soil conservation service curve number (SCS-CN) methodology introduction. *Journal of Hydrologic Engineering, 17*(11), 1157-1157.

MRC, 2011. The Flood Management and Mitigation Program 2011–2015. Mekong River Commission, Phnom Penh, Cambodia.

Mtamba, J., Velde, R. V. D., Ndomba, P., Zoltán, V., & Mtalo, F. (2015). Use of Radarsat-2 and Landsat tm images for spatial parameterization of manning's roughness coefficient in hydraulic modeling. *Remote Sensing, 7*(1), 836-864.

Neal, J., Schumann, G., & Bates, P. (2012). A subgrid channel model for simulating river hydraulics and floodplain inundation over large and data sparse areas. *Water Resources Research, 48*(11), 11506.

Nguyen, P., Thorstensen, A., Sorooshian, S., Hsu, K., Aghakouchak, A., & Sanders, B., et al. (2015). A high resolution coupled hydrologic–hydraulic model (HiResFlood-UCI) for flash flood modeling. *Journal of Hydrology, 541,* 401-420.

Paiva, R. C. D. D., Buarque, D. C., Collischonn, W., Bonnet, M. P., Frappart, F., & Calmant, S., et al. (2013). Large-scale hydrologic and hydrodynamic modeling of the Amazon River basin. *Water Resources Research, 49*(3), 1226–1243.

Pantaleoni, E., Engel, B. A., & Johannsen, C. J. (2007). Identifying agricultural flood damage using Landsat imagery. *Precision Agriculture, 8*(1), 27-36.

Samantaray, D., Chatterjee, C., Singh, R., Gupta, P. K., & Panigrahy, S. (2015). Flood risk modeling for optimal rice planning for delta region of Mahanadi river basin in India. *Natural Hazards, 76*(1), 347-372.

Sanders, B. F. (2007). Evaluation of on-line DEMs for flood inundation modeling. *Advances in Water Resources, 30*(8), 1831-1843.

Satir, O., & Berberoglu, S. (2016). Crop yield prediction under soil salinity using satellite derived vegetation indices. *Field Crops Research, 192*, 134-143.

Schmidhuber, J., & Tubiello, F. N. (2007). Global food security under climate change. *Proceedings of the National Academy of Sciences*, *104*(50), 19703-19708.

Schumann, G. J. P., Bates, P. D., Neal, J. C., & Andreadis, K. M. (2014). Technology: fight floods on a global scale. *Nature, 507*(7491), 169.

SCS, 1956. National Engineering Handbook, Hydrology, Section 4, Soil Conservation Service, US Department of Agriculture, Washington, DC.

Tarekegn, T. H., Haile, A. T., Rientjes, T., Reggiani, P., & Alkema, D. (2010). Assessment of an ASTER-generated DEM for 2D hydrodynamic flood modeling. *International Journal of Applied Earth Observation & Geoinformation, 12*(6), 457-465.

Thornton, P. K., Ericksen, P. J., Herrero, M., & Challinor, A. J. (2014). Climate variability and vulnerability to climate change: a review. *Global Change Biology*, *20*(11), 3313-3328.

Tucker, C. J. (1979). Red and photographic infrared linear combinations for monitoring vegetation. *Remote Sensing of Environment*, *8*(2), 127-150.

UNDP, 2004. Reducing Disaster Risk: A Challenge for Development. UNDP, New York, USA.

Vozinaki, A. E. K., Karatzas, G. P., Sibetheros, I. A., & Varouchakis, E. A. (2015). An agricultural flash flood loss estimation methodology: the case study of the Koiliaris basin (Greece), February 2003 flood. *Natural Hazards, 79*(2), 899-920.

Wang, Q., Wu, C., Li, Q., & Li, J. (2010). Chinese HJ-1A/B satellites and data characteristics. *Science China Earth Sciences*, *53*, 51-57.

Woodward, D., Hawkings, R., Hjelmfelt, A., Van Mullen, J., & Quan, Q., 2002. Curve Number method: origins, applications and limitations. Second Federal Interagency Hydrologic Modeling Conference, Las Vegas, Nevada

Xia, J., Falconer, R. A., Lin, B., & Tan, G. (2011). Numerical assessment of flood hazard risk to people and vehicles in flash floods. *Environmental Modelling & Software, 26*(8), 987-998.

Xia, X., & Liang, Q. (2016). A GPU-accelerated smoothed particle hydrodynamics (SPH) model for the shallow water equations. *Environmental Modelling & Software, 75*, 28-43.

Xue, J., & Su, B. (2017). Significant Remote Sensing Vegetation Indices: A Review of Developments and Applications. *Journal of Sensors, 2017*.

Zhang, J., Feng, L., & Yao, F. (2014). Improved maize cultivated area estimation over a large scale combining MODIS–EVI time series data and crop phenological information. *ISPRS Journal of Photogrammetry and Remote Sensing*, *94*, 102-113.

Zhang, S., & Pan, B. (2014). An urban storm-inundation simulation method based on GIS. *Journal of Hydrology, 517*(5), 260–268.

Zhang, X., & Zhang, Q. (2016). Monitoring interannual variation in global crop yield using long-term AVHRR and MODIS observations. *ISPRS Journal of Photogrammetry & Remote Sensing, 114*, 191-205.

Zhong, L., Hu, L., Yu, L., Gong, P., & Biging, G. S. (2016). Automated mapping of soybean and corn using phenology. *ISPRS Journal of Photogrammetry & Remote Sensing, 119*, 151-164.

## Figure Captions:

**Fig. 1.** The study area

**Fig. 2.** Evaluation system of agricultural flood impact using remote sensing imagery and two-dimensional hydraulic model

**Fig. 3.** Distribution of spring corn, rice and soybean in Jilin Province

**Fig. 4.** The validation of the crop classification area (Y-axis) against the official crop county-level, planted area statistics (X-axis)

**Fig. 5.** Correlation between actual and predicted yields for (a) spring corn in 2013; (b) spring corn in 2014; (c) rice in 2013; (d) rice in 2014; (e) soybean in 2013; and (f) soybean in 2014

**Fig. 6.** The predicted yield for (a) spring corn in 2013; (b) spring corn in 2014; (c) spring corn in 2013 versus 2014; (d) rice in 2013; (e) rice in 2014; (f) rice in 2013 versus 2014; (g) soybean in 2013; (h) soybean in 2014; and (i) soybean in 2013 versus 2014

**Fig. 7.** Flood simulation results for the headwater watershed of the Dongliao River

**Fig. 8.** Flood simulation results for the headwater watershed of the Mudanjiang River

**Fig. 9.** Velocity-loss functions for spring corn, rice and soybean

**Table 1. Yield loss correlations with flood characteristics by crop type**

| Crop | Water depth | | Flow velocity | | Duration at depth > | | |
|---|---|---|---|---|---|---|---|
| | Maximum | Mean | Maximum | Mean | 5cm | 10cm | 20cm |
| Spring corn | -0.56 | -0.62 | -0.86 | -0.85 | -0.28 | -0.38 | -0.51 |
| Rice | -0.24 | -0.30 | -0.77 | -0.78 | -0.14 | -0.21 | -0.31 |
| Soybean | -0.11 | -0.09 | -0.62 | -0.70 | -0.28 | -0.39 | -0.51 |

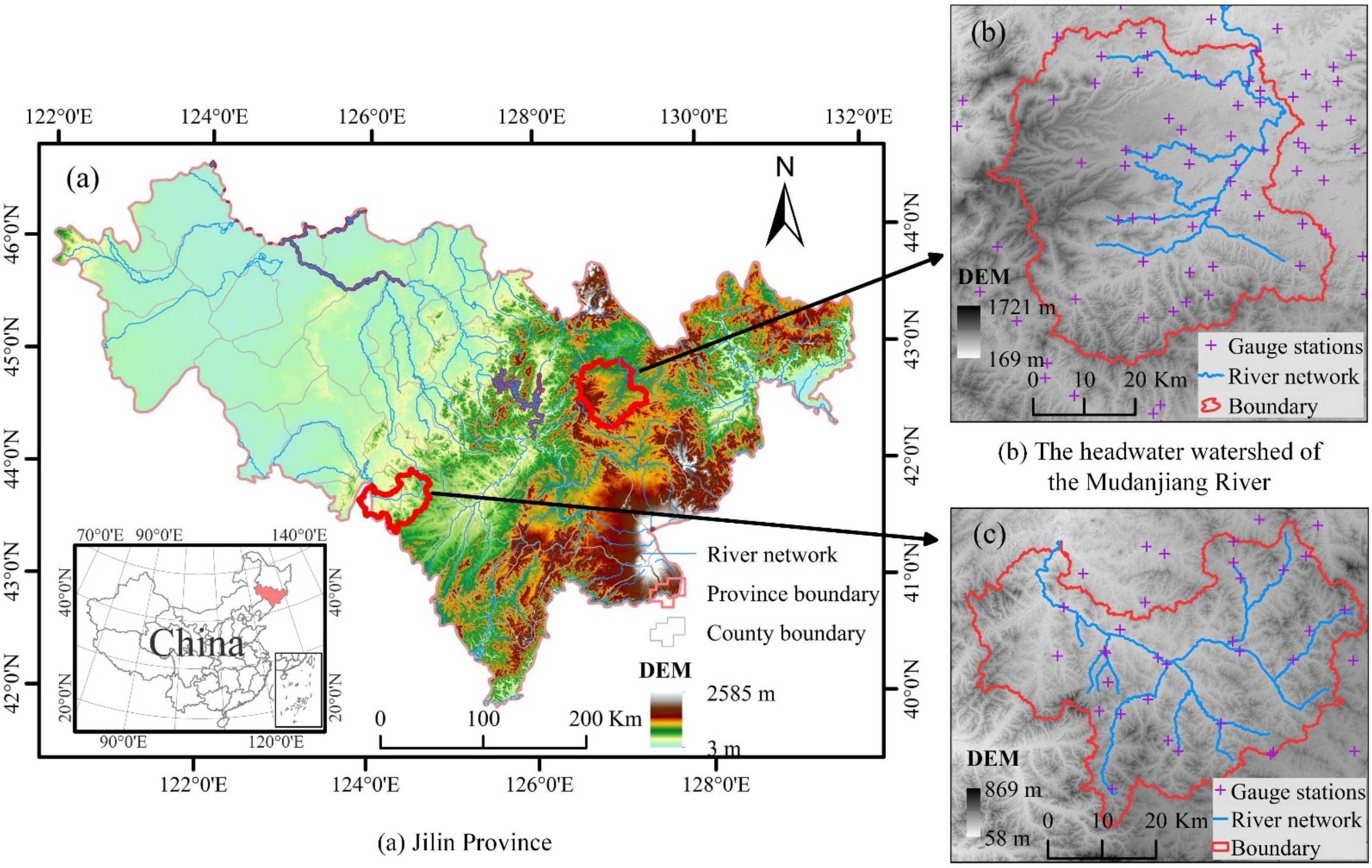

(a) Jilin Province

(b) The headwater watershed of the Mudanjiang River

(c) The headwater watershed of the Dongliao River

**Fig. 1. The study area**

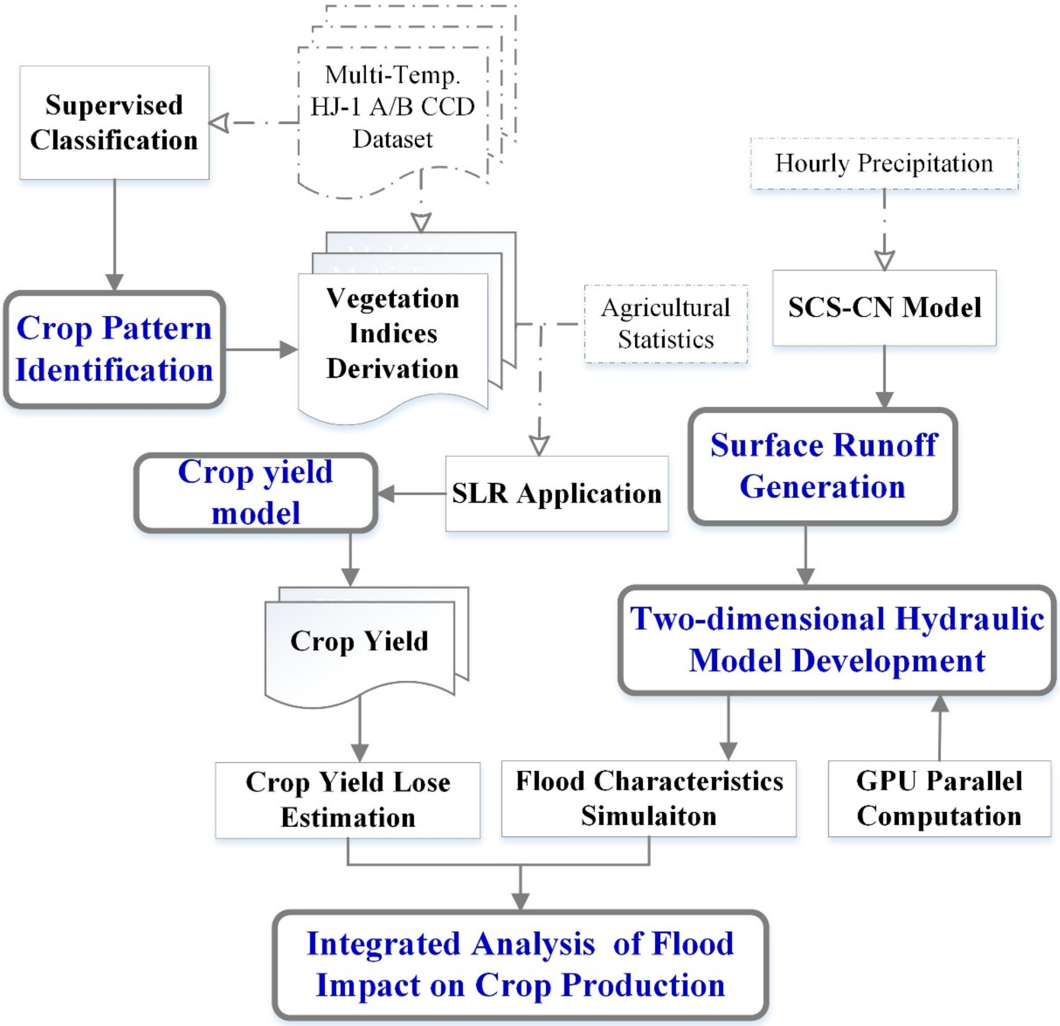

**Fig. 2. Evaluation system of agricultural flood impact using remote sensing imagery and two-dimensional hydraulic model**

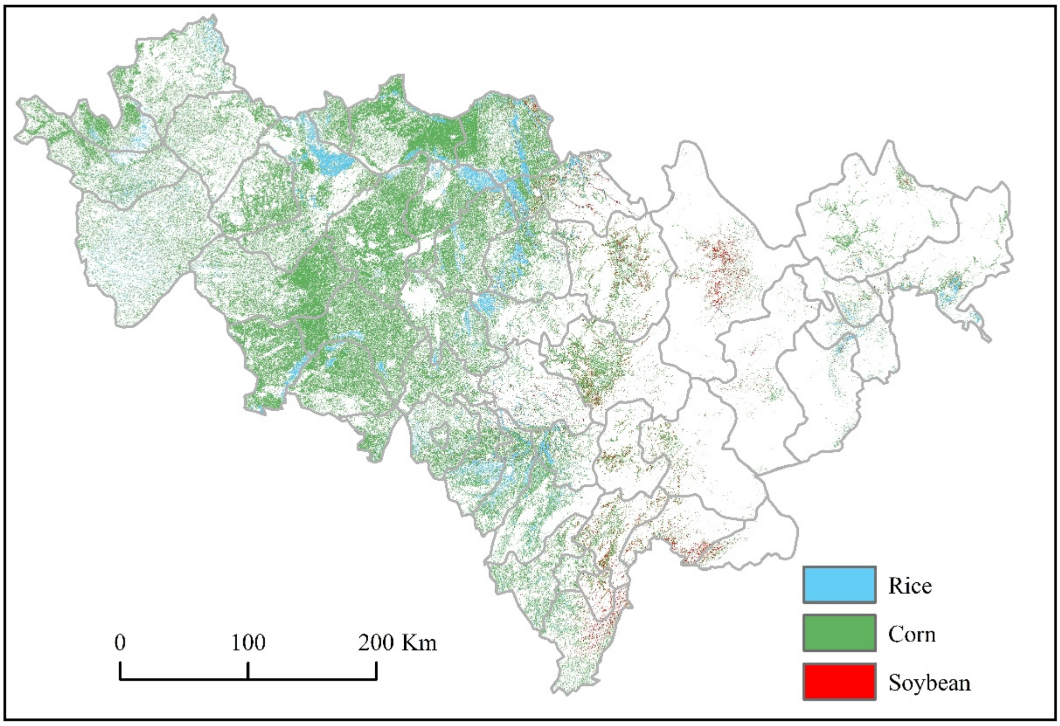

Fig. 3. Distribution of spring corn, rice and soybean in Jilin Province

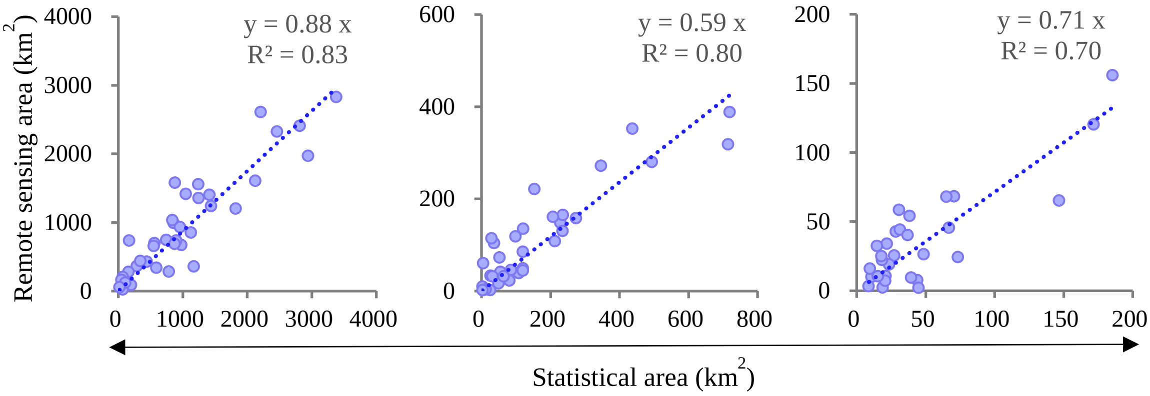

(a) Spring corn (b) Rice (c) Soybean

**Fig. 4. The validation of the crop classification area (Y-axis) against the official crop county-level, planted area statistics (X-axis)**

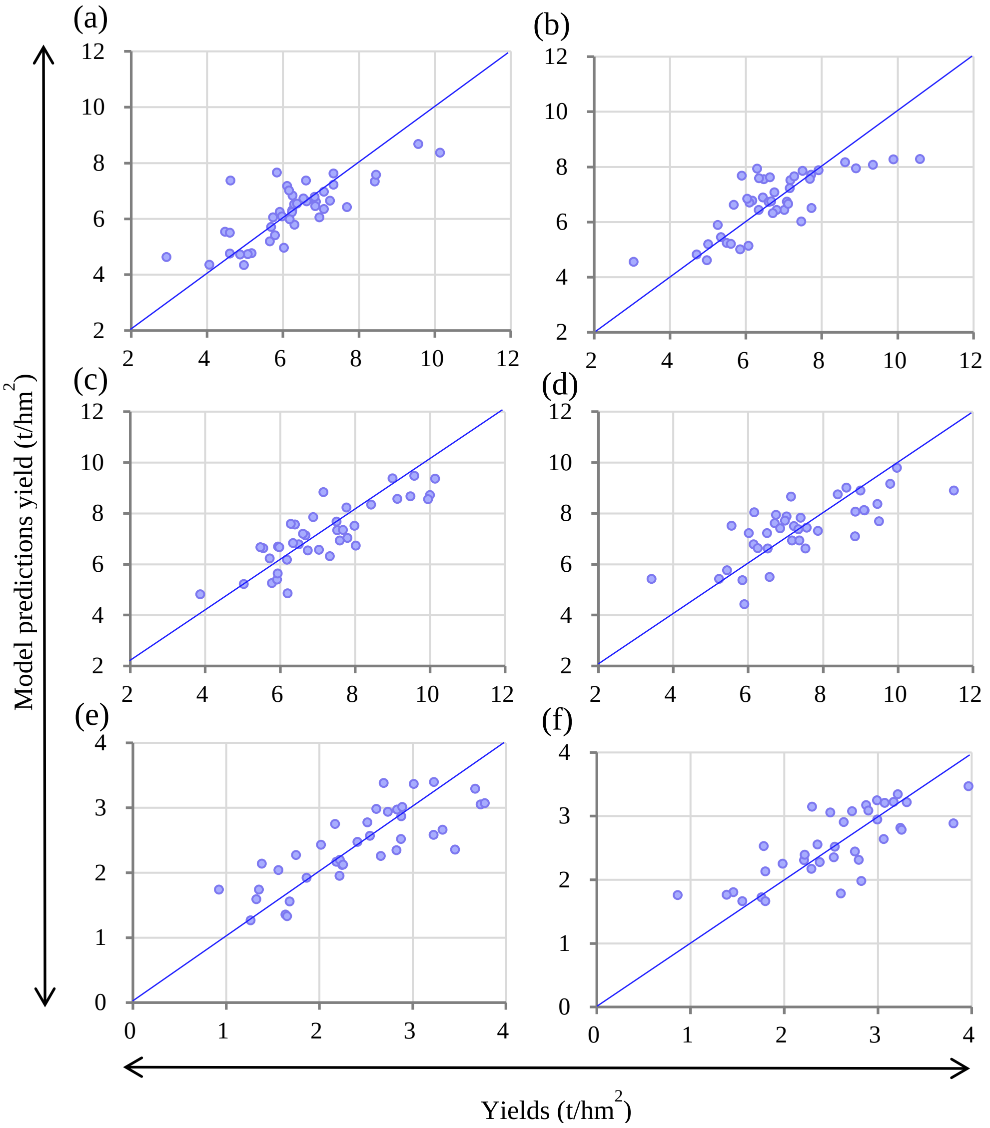

**Fig. 5. Correlation between actual and predicted yields for (a) spring corn in 2013; (b) spring corn in 2014; (c) rice in 2013; (d) rice in 2014; (e) soybean in 2013; and (f) soybean in 2014**

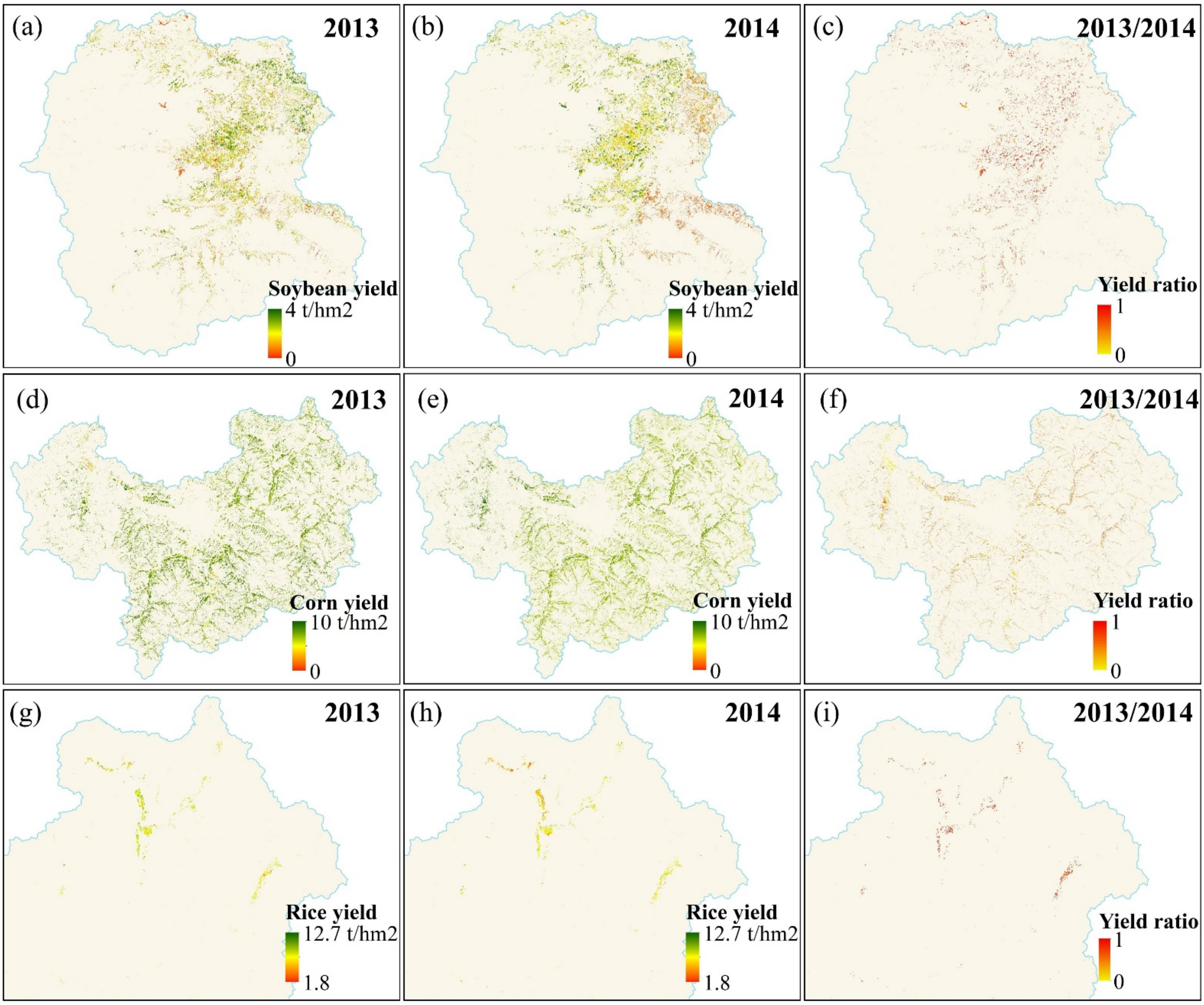

**Fig. 6. The predicted yield for (a) spring corn in 2013; (b) spring corn in 2014; (c) spring corn in 2013 versus 2014; (d) rice in 2013; (e) rice in 2014; (f) rice in 2013 versus 2014; (g) soybean in 2013; (h) soybean in 2014; and (i) soybean in 2013 versus 2014**

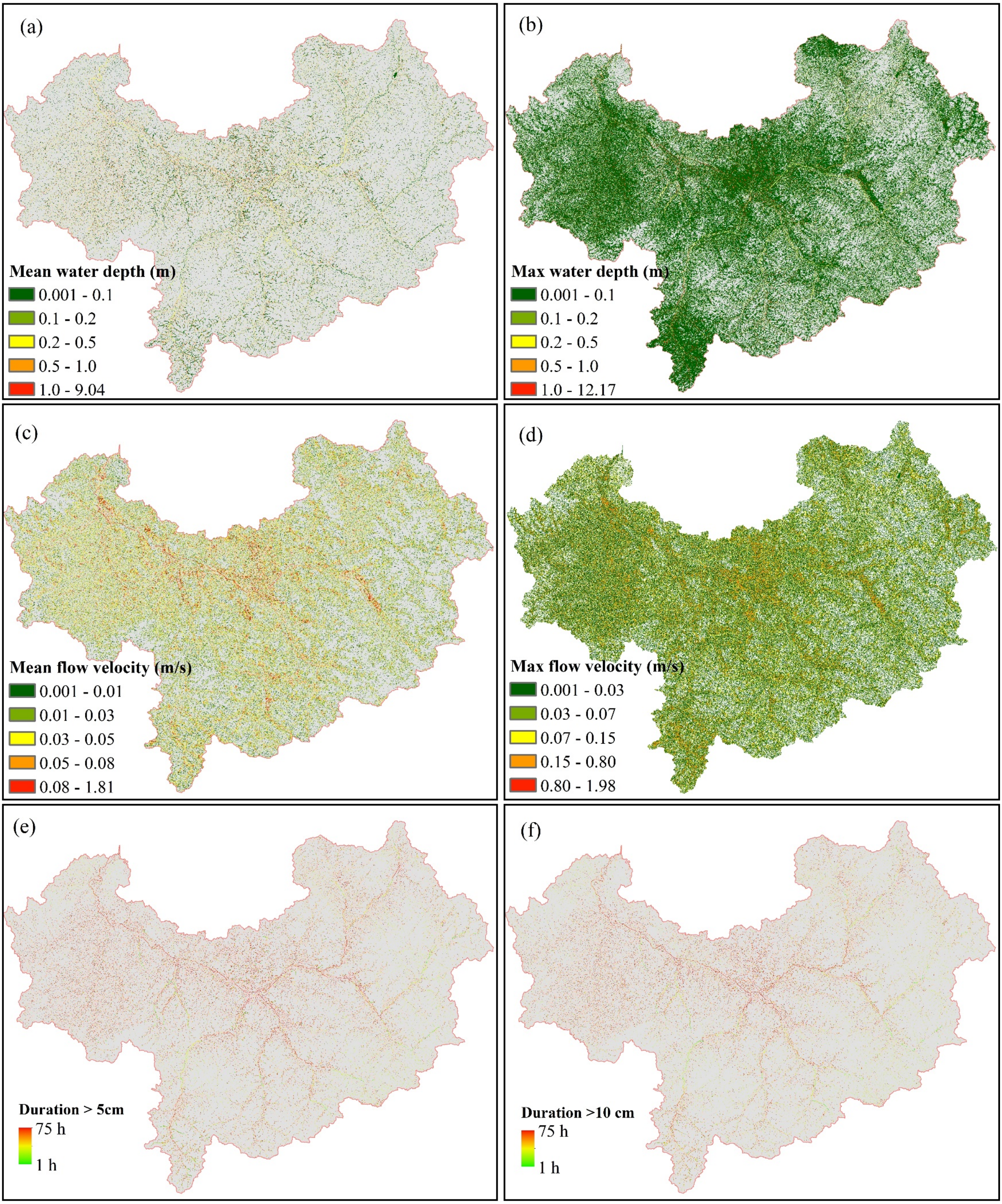

**Fig. 7. Flood simulation results for the headwater watershed of the Dongliao River**

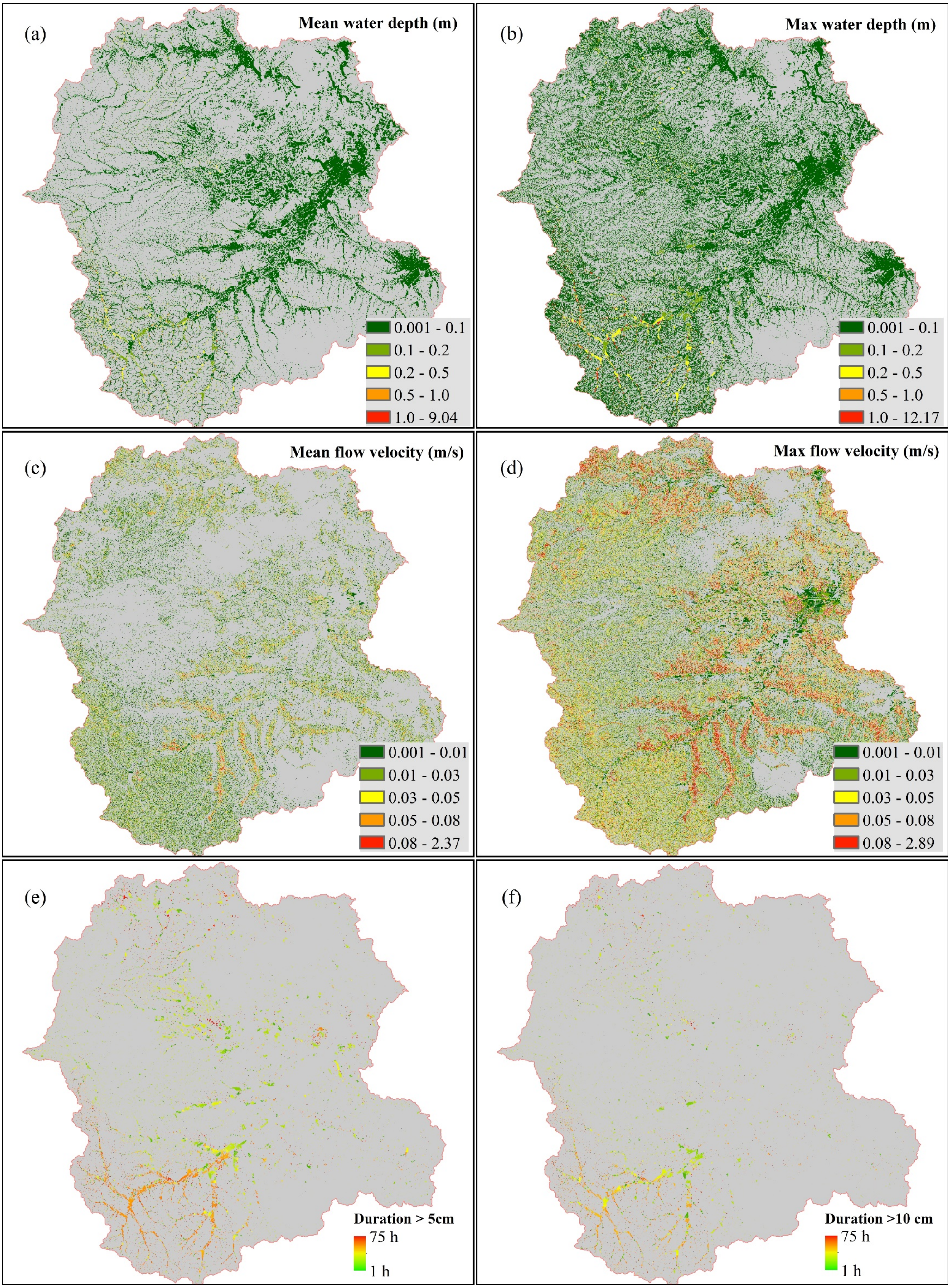
(a)
Mean water depth (m)
0.001 - 0.1
0.1 - 0.2
0.2 - 0.5
0.5 - 1.0
1.0 - 9.04
(b)
Max water depth (m)
0.001 - 0.1
0.1 - 0.2
0.2 - 0.5
0.5 - 1.0
1.0 - 12.17
(c)
Mean flow velocity (m/s)
0.001 - 0.01
0.01 - 0.03
0.03 - 0.05
0.05 - 0.08
0.08 - 2.37
(d)
Max flow velocity (m/s)
0.001 - 0.01
0.01 - 0.03
0.03 - 0.05
0.05 - 0.08
0.08 - 2.89
(e)
Duration > 5cm
75 h
1 h
(f)
Duration >10 cm
75 h
1 h

**Fig. 8. Flood simulation results for the headwater watershed of the Mudanjiang River**

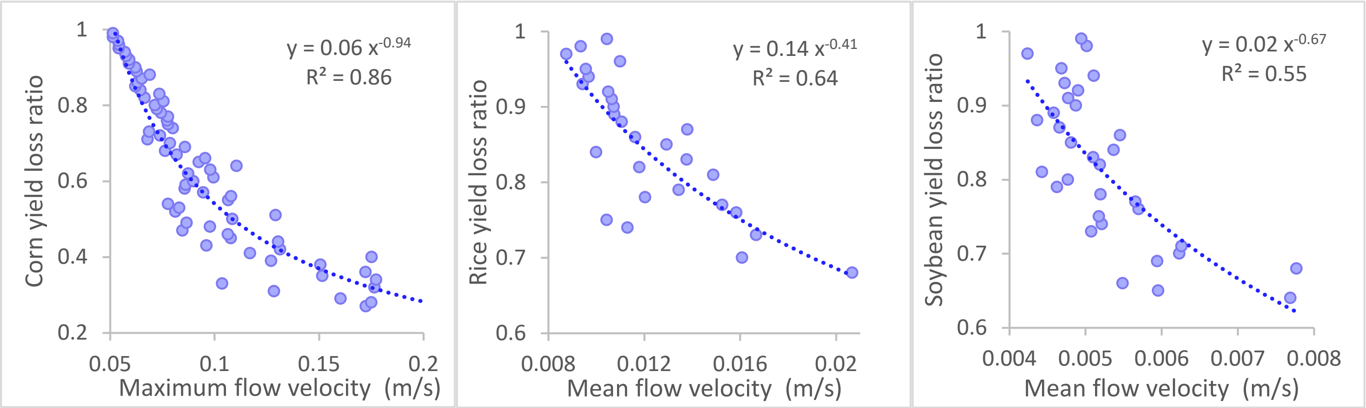

(a) Spring corn (b) Rice (c) Soybean

**Fig. 9. Velocity-loss functions for spring corn, rice and soybean**